Effects of Strake Coverage and Marine Growth on Flexible Cylinder VIV

Proceedings of the ASME 2014 33rd International Conference on Ocean, Offshore and Arctic Engineering
OMAE2014
June 8-13, 2014, San Francisco, California, USA

OMAE2014-24462

EFFECTS OF STRAKE COVERAGE AND MARINE GROWTH ON FLEXIBLE CYLINDER VIV

Themistocles L. Resvanis
Massachusetts Institute of Technology
Cambridge, MA, USA

Zhibiao Rao
Massachusetts Institute of Technology
Cambridge, MA, USA

J. Kim Vandiver
Massachusetts Institute of Technology
Cambridge, MA, USA

ABSTRACT

In this paper we present some results from the recent SHELL tests at the MARINTEK basin. The tests involved towing densely instrumented flexible cylinders at Reynolds numbers up to 220,000. The main objective is to present the experimental results describing the effectiveness of different amounts of strake coverage and to explore the influence of simulated marine growth.

The data is presented in terms of CF response amplitudes and rainflow-counted damage rates due to the combined CF and IL bending stresses. All results are compared with the bare cylinder cases which will be used as a reference to determine how effective the strakes are in suppressing VIV and how this effectiveness can be affected by marine growth. The results show that even small bare sections (missing strakes) can lead to significant VIV response. We also observe that moderate amounts of marine growth can quickly negate any suppression coming from the strakes.

INTRODUCTION

As oil and gas exploration and production moves into deeper and deeper waters, the fatigue damage accumulated due to Vortex-Induced Vibrations (VIV) is quickly becoming one of the most critical aspects of deep-water riser design. Helical strakes and other suppression devices are commonly used to try and minimize the effects of VIV. They work by ensuring that the flow separation points are not aligned along the structure or by moving the reattachment points further downstream of the cylinder, in any case they interrupt the coherence of the shed vortex sheet thus minimizing the power into the structure.

Over the past years several strake and fairing designs have been proven to be extremely effective in disrupting VIV on rigid or fully covered flexible cylinders. The question that remains to be answered is how much strake coverage is actually necessary to minimize VIV on a flexible cylinder or conversely; how many strakes can one lose before VIV becomes a serious source of fatigue damage on the now partially straked riser.

The other pressing issue that needs to be addressed once a strake design and coverage has been chosen is to determine how the suppression characteristics of the chosen device will be affected by the inevitable presence of marine growth. This might be done in order to determine a cleaning schedule or to simply account for the accumulated damage so that one has more confidence in the design or future operation of the riser.

This work makes use of test data gathered on behalf of SHELL International Exploration and Production Co. by MARINTEK. The tests involved towing three different 38m long flexible pipes/cylinders in uniform and sheared currents with different suppressions devices, amounts of strake coverage and simulated marine growth.

In the first part of this paper we propose a framework/methodology for experimentally determining the worst possible combination of Cross-Flow (CF) and In-Line (IL) damage, i.e. we calculate the position around the circumference of the cylinder's cross-section that will experience the most severe loading due to the simultaneous motion in both CF and IL directions. The analysis shows that the damage due to the IL motion is comparable to that of the CF motion, and their combined effect results in a damage rate of the same order of magnitude as the pure CF signal and is usually situated at a position around the circumference of the cross-section that is very close to or coincides with the CF direction.

The second part of this paper focuses on how effectively four different strake coverage amounts suppress VIV (always using the same strake design). The data is presented in terms of response amplitudes and damage rates, and it is demonstrated that the much larger reduction in damage rate is

primarily due to the elimination of higher harmonics rather than simply being the result of smaller response amplitudes.

Finally the tests analyzing the effects of simulated marine growth demonstrate how even small amounts of marine growth can quickly alter the efficiency of a specific strake design and lead to damage rates and accumulated fatigue that is many times higher than that expected with clean strakes.

DESCRIPTION OF EXPERIMENTS

The 38m SHELL experiments were conducted at MARINTEK's ocean basin on behalf of SHELL International Exploration and Production Co. The experiment involved testing three densely instrumented cylinders of different diameters. The flexible cylinders were mounted under a carriage that could traverse the basin in a manner capable of simulating both uniform and linearly sheared flows. The full test matrix included runs which tested the effects of fairings, strakes, staggered buoyancy and marine growth on riser response. A most interesting feature of this data set was the very large range of Reynolds numbers covered while testing the three different pipes. Towing velocities ranged from 0.25m/s to 3.45m/s which correspond to a Reynolds number range from 5,000 to 220,000. More details on the experimental set-up can be found in [1&4].

This work focus on analyzing only the data obtained for the response of the largest diameter model. The cylinder properties are summarized in *Table 1*.

Table 1. Pipe Properties

Length	38 m
Outer Diameter (Hydrodynamic Dia.)	80 mm
Optical Diameter (Strength Dia.)	27 mm
Inner Diameter	21 mm
EI	572.3 Nm^2
E	3.46e10 N/m^2
Mass in air (with contents)	5.708 kg/m
Mass in water (with contents)	0.937 kg/m
Mass ratio	1.14

The pipe had fiber optic Bragg strain gauges at 30 different locations and accelerometers at 22 locations along the span in both the CF and IL directions. The curvature/strain was measured at a distance of 13.5mm from the neutral axis and all sensors were sampled at a rate of 1200Hz. Damping tests, conducted in air, yielded structural damping ratios of ~0.5-0.7% of critical.

The triple start helical strakes were made from polyurethane and were delivered in sections 0.43m long. Each section was made of two halves which were 'clamped' around the cylinder and held together with zip-ties. The strake design called for a fin height equal to 25% of the outer diameter and a pitch equal to 15 diameters.

A small gap was left between every five buoyancy modules, such that the coverage would be similar to the best that could be done on a typical marine riser with connectors. This resulted in a ~83% effective coverage. This will be referred to as the fully covered case.

After testing the cylinder while it was fully covered with strakes, the test matrix called for removing sections of strakes from the mid-span in order to create continuous bare gaps equal to 5%, 15%, 25% and 50% of the model's length. *Figure 1* is a photograph showing the strake design and a small bare section.

Fig.1 Straked and bare sections.

The marine growth was only applied on the fully straked cylinder (83% coverage). The carpeting used to simulate soft marine growth had two different heights corresponding to 30% and 60% of the fin height. It is important to note that the marine growth was only applied around the circumference of the cylinder and not on the fins themselves, as shown in *Figure 2*.

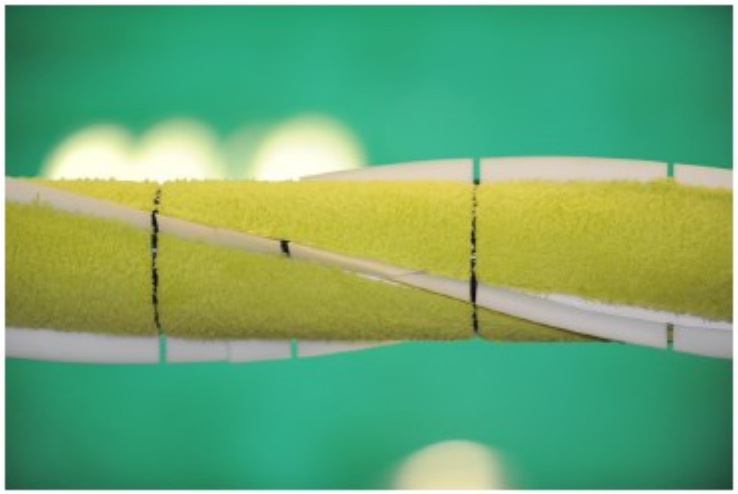

Fig. 2 Strakes with simulated soft marine growth

Table 2 summarizes all the test cases used in the analysis presented in this paper. The table lists the strake coverage/configuration, whether marine growth was applied and the range of towing velocities tested in both uniform and sheared flows for each configuration.

Table 2. Test Matrix of Cases Used in Present Analysis

Strake Configur.	*Marine Growth*	*Uniform-Flow Speeds (m/s)*	*Sheared-Flow Speeds (m/s)*
BARE	NONE	0.5-1.8	0.5-3.0
50% gap	NONE	0.25-1.5	N.A.
25% gap	NONE	0.25-1.5	N.A.

15% gap	NONE	0.25-1.5	N.A.
5% gap	NONE	0.25-1.5	N.A.
FULL STRAKE COVERAGE	NONE	0.25-1.5	N.A.
	30% high	0.25-1.5	0.25-2.5
	60% high	0.25-1.5	0.25-2.5
	30% high, only between 0<x/L<0.4	N.A.	0.25-2.5

DATA ANALYSIS

Many of the data processing techniques used in this work are fairly standard in the VIV model-testing community and many more details can be found in [2 & 3]. Data analysis procedures will only be briefly discussed here to the extent necessary for a reader to understand where the data presented in later sections originated.

The amplitude at every accelerometer location was determined after double-integrating the accelerometer time histories in the frequency domain. To account for the possibility that the location where the maximum response occurs falls between two measurement locations, a modal reconstruction was performed using both the available curvature response data and the amplitude data.

Response spectra where typically obtained by averaging the information from several neighboring curvature sensors. All time-series were high-pass filtered to remove any mean/static components that are not particularly relevant to VIV analysis, but unless otherwise noted, all higher harmonics were taken into account.

NEED FOR RAINFLOW-COUNTING

It is conceivable that due to the complicated motion of the cylinder while undergoing VIV, the most damaging location around the circumference of the cross-section does not coincide with the CF or IL directions but rather at some angle between the two.

In this paper we propose calculating the stresses and damage rates at 24 positions (*i=1,2...,24)* around the circumference of the cross-section as shown in *Figure 3*. This will be done at every sensor location along the pipe length.

At each circumferential position, the stress time history, $\sigma_{\theta i}$, is given by the appropriate vector addition of the CF and IL stress signals, σ_{CF} and σ_{IL} respectively.

$$\sigma_{\theta_i}(t) = \sigma_{CF}(t)\cos(\theta_i) + \sigma_{IL}(t)\sin(\theta_i) \qquad eq.\ 1$$

Figure 4 shows the results of this vector addition and the resulting stress time histories at the angles corresponding to θ=0 (i.e. CF), θ=30°, θ=60°, θ=90° (i.e. IL). This is done at every angle, θ_i, and each stress time-history is subsequently rain-flow counted, and the most damaging position/angle is chosen as the *combined stress* or *combined damage* for each one of the 30 locations along the length of the pipe where the CF and IL strain gauges are located.

The main motivation for combining the stress components in such a way is the profound importance that frequency content has on the damage rate/fatigue calculations. The idea is based on the analysis presented in [5], the main difference being that in this work we will rain-flow count all the time histories whereas the authors in [5] calculated a damage index based on the RMS stresses for both the CF and IL directions and their respective response frequencies and only then applied the coordinate transformation similar to *Equation 1* to their RMS quantities.

Estimating the fatigue life (or Damage Rate) for a perfectly sinusoidal stress time history is straightforward since the analytic equations are straightforward to derive. Similarly, if the stress time-history is narrow banded Gaussian once again the analytic expressions for Damage Rate can be derived as shown in [6]. If the signal contains multiple frequencies and the response amplitude varies significantly, one has no other choice except to revert to cycle counting. Cycle counting algorithms essentially try to apply Miner's law by examining every half-oscillation in a time history and by placing it in bins according to the amplitude of the examined half-cycle.

From *Figure 4* it should be apparent that after applying the coordinate transformation given by *equation 1* we obtain stress time-histories that contain multiple frequencies and a lot of variability in the amplitude. As such, in this paper we will be using the rain-flow counting algorithm as implemented in the WAFO toolbox [7] in order to measure the actual damage accumulated by the cylinder during each test.

Since fatigue properties are not available for the exact composite material that the flexible cylinder was made of, all fatigue calculations will assume that it was made of steel with an S-N curve defined according to the DNV-F curve (i.e. log(a)=11.378 and m=3.0 [12]).

Figure 5 shows the response of the fully bare pipe under a uniform flow excitation of 1.4 m/s. The top plot shows the CF and IL displacements as calculated by the modal reconstructions. Observe that even though the IL response amplitude is much smaller, there are certain locations where the IL stresses are of comparable magnitude with the CF stresses! This happens because even though the IL response amplitude is significantly smaller than the CF amplitude, the IL wavenumber is much greater than the CF wavenumber due to the approximately two times higher response frequency. The relationship between stresses and amplitude for a flexural wave on a beam is shown in *Equation 2*. Here, σ is a stress, E is the Young's Modulus, ε is the bending related strain, *A* is the response amplitude at a specific time instant, *OD/2* is the distance from the neutral axis at which the stresses/strains were measured (13.5mm) and *k* is the wavenumber.

$$\sigma = E\varepsilon = EA\frac{OD}{2}k^2 \qquad eq.\ 2$$

Figure 5 also shows the damage rate along the length of the pipe. Each location has two data-points corresponding to the damage rates as calculated from the CF and IL stress time-histories and a third data-point corresponding to the damage rate from the most damaging combination of the CF and IL stress time histories according to *Equation 1*. The last plot shows the angle around the circumference of the cross-section at which the most damaging combination of CF and IL occurred. Note that even though the combined damage rate at most sensor locations tends to coincide with the CF direction there are a few locations where this is not the case.

RESULTS AND DISCUSSION

BARE PIPES

Figure 6 shows the maximum damage rate along the pipe span as a function of towing speed for the uniform flow tests. For each test/flow speed there are three values: the CF and IL directions as well as the most damaging combination of the two. Similarly, *Figure 7* shows the maximum damage rates for the sheared flow tests. For both uniform and sheared flow tests we see that the IL rate is the same order of magnitude as the CF. Note that the worst possible combination of the two coincides or is virtually identical to the CF damage calculation suggesting that the most damaging position around the circumference tends to be at or very close to the CF direction This is also demonstrated for a specific test in the last plot of *Figure 5*.

The stress signals used for plotting *Figures 6 & 7*, contained large amounts of higher harmonics (3X and 5X for the CF and 4X for the IL directions) as is typically observed in high mode number model testing.

Figures 8 & 9 show what would happen if the CF and IL signals had been band-pass filtered around the 1X and 2X frequencies respectively. Very similar trends are observed with the exception that now there are a few cases where the worst possible damage calculation around the cross-section coincides with the IL signal/direction. This happens because the CF signal no longer includes the 3X and 5X components which greatly affect the damage rate due to their high frequencies.

In any case, we see that the worst possible damage rate around the circumference of the cross-section and the IL damage rate are always of the same order of magnitude as the CF damage rate.

The aim of this section was not to dismiss the importance of IL motion, to the contrary, we wanted to carefully measure the fatigue caused by the IL motion and demonstrate experimentally that the worst possible damage accumulated anywhere around the cross-section is very close to the CF damage rate. If one can **conservatively** design for cross-flow VIV, then one should be confident that they have accounted for the worst possible case of combined CF and IL VIV. The authors find that this is especially interesting in light of the recent DEEPSTAR *Factor of Safety* papers [8 & 9], where experimentally measured CF damage rates were compared with results from VIV response prediction software that, to date, only account for CF VIV.

STRAKE COVERAGE

As discussed earlier four different partial strake coverages were tested in this set of experiments. *Figure 10,* compares the effectiveness of these different coverage amounts in suppressing VIV by comparing the CF amplitude with that of the fully bare cylinder as a function of towing velocity (or current speed). Similarly, *Figure 11* compares the maximum damage rate along the cylinder with that recorded for the bare cylinder. The damage rate reported is that due to the worst possible combination of CF and IL motion according to methodology described earlier, however this tends to coincide with the CF direction due to the very small IL motion that results after adding the strakes.

Observe, that the reduction in damage rate is much more dramatic than the reduction of amplitude for a given strake coverage. The reasons for this become obvious after examining a typical response spectrum (PSD) for the partial strake coverage tests. *Figure 12*, shows the averaged PSD of all CF strain gauges along the length of the pipe when the flow speed was 1m/s. Four different lines are plotted for the bare, 50% and 25% long bare gaps in the middle as well as the fully straked cases. Note how the 3X and 5X peaks for the partial strake coverage cases are greatly reduced when compared to the bare cylinder case. In fact the fully straked case manages to suppress the higher harmonics entirely.

The resulting reduction in amplitudes and damage rates is due to the following reasons:

- The presence of straked sections will tend to restrict the power-in regions to the bare sections only. This has the effect of reducing the length of the pipe available for power input to the structure and simultaneously increasing the power out of the structure by allowing a portion of the structure to contribute to the hydrodynamic damping [10].
- Straked sections that belong to the power-out regions will contribute more to the hydrodynamic damping than a bare section of similar length [11].

The above reasons, are really only applicable to strake configurations with sizeable bare sections. For the fully straked cases and the cases with 5% long bare sections in the middle, examination of the spectra revealed that the excitation is being driven entirely by the straked sections. In these situations, the VIV amplitude and damage rates are very small because of the very small lift coefficient provided by the lack of span-wise coherence of the wake. As mentioned previously the very small damage rates measured are due to a combination of very small response amplitudes and negligible higher harmonics present.

Even though the same very efficient strake design was used in all the different configurations we see that the CF VIV amplitude is virtually minimized only for the fully strake covered arrangement and the configuration with a small bare gap only 5% long. This is an important result to keep in mind when applying strakes to flexible cylinders. In reality it is not sufficient to solely talk about ‘strake efficiency’ unless the effectiveness of the proposed strake coverage/distribution is also addressed.

The concept of ‘strake efficiency’ should really be applicable (or reserved) for straked rigid cylinders and fully covered flexible cylinders in uniform flows, since the same strakes are not ‘effective’ in suppressing VIV if they do not cover the entire structure or at the very least what would have been the power-in regions.

Furthermore, defining ‘efficiencies’ simply in terms of response amplitude overlooks the fact that strakes suppress higher harmonics thus greatly contributing to the fatigue life by eliminating the high frequency components.

MARINE GROWTH

Figure 13 reveals the profound effect that marine growth can have on the VIV suppression effectiveness. The figure is a plot of the maximum damage rate along the span vs. current speed in uniform flows for the two different amounts of

simulated marine growth tested. The figure also includes the bare pipe and the clean, fully strake covered results which, as would be expected, bracket the response.

The addition of marine growth between the strake's fins essentially reduces their height making them less efficient. By the time the marine growth has covered 60% of the fin height the cylinder cross-section starts resembling a cross-section of larger effective diameter with short and stubby fins. This is evident from the spectra in *Figure 14* where it is clear that the response frequency has shifted down with the addition of the simulated marine growth. The plot shows the response spectrum as calculated from the average of all 30 CF strain gauges.

Figure 15 shows the effect of marine growth on fully straked cylinders exposed to sheared flows. This figure also includes the very interesting case of a fully straked riser with marine growth (60% high) only applied in the region $0<x/L<0.6$, i.e. the high speed end. This situation is very similar to what happens in the ocean where marine growth affects only the upper portion of a very long submerged structure.

Note, how even though only a portion of the straked cylinder is covered in marine growth the response is very similar to that of the cylinder fully covered in marine growth of the same height. This happens, because in both situations there is marine growth at the high speed end, which is always the power-in region under linearly sheared flows [10]. The slightly lower response at certain speeds, of the cylinder partially covered in marine growth could be explained by the fact that the clean strakes which are located in the power-out region provide more hydrodynamic damping than the marine growth covered strakes.

CONCLUSIONS

The first part of this work proposes a framework for determining the magnitude and location of the most damaging combination of CF and IL bending strain around the circumference of the pipe's cross-section. The results show that this usually occurs at or very close to the pure CF direction. In any case, the most damaging combination of CF and IL stress, in terms of damage rate, is usually very similar in magnitude to the pure CF damage rate and always of the same order of magnitude. This is very reassuring since most VIV analysis only accounts for damage due to CF motion.

The second and main part of this work focuses on the effectiveness of different amounts of strake coverage. It is demonstrated that the concept of 'strake efficiency' is practically useless in predicting what will happen in the context of flexible cylinders perhaps with the exception of an idealized case of full strake coverage in uniform flows. The results show that even though the tests used an extremely well designed strake from a hydrodynamic standpoint, a bare section, just 15% of the total length, is sufficient to result in noticeable VIV under uniform flow conditions.

Additionally the tests showed that a reduction of response amplitude of one order of magnitude will have an associated reduction in damage rate that is several times larger because of the ability of strakes to suppress the 3X and 5X higher harmonics.

Finally, the experiments demonstrated that even small amounts of marine growth, equal to 30% of the strake's fin height, are sufficient to increase the measured damage rates by an order of magnitude compared to clean strakes. Modest amounts of marine growth, equal to 60% of the fin height, are capable of negating most of the suppression benefits provided by clean strakes by increasing the measured damage rates by more than two orders of magnitude.

ACKNOWLDEGEMENTS

The authors acknowledge SHELL International Exploration and Production Co. for providing access to the experimental data and the SHEAR7 JIP members (BP, Chevron, ConocoPhillips, ExxonMobil, Petrobras, Shell, Statoil & Technip) for supporting this research.

REFERENCES

[1] MARINTEK, 2011, *Shell Riser VIV Tests Main Report*, No. 580233.00.0

[2] Resvanis, T.L. et al., 2012, *Reynolds Number Effects on the Vortex-Induced Vibration of Flexible Marine Risers*, OMAE2012-83565

[3] Rao, Z. et al, 2012, *The Effect of Exposure Length on the Vortex Induced Vibration of Flexible Cylinders*, OMAE2012-83272

[4] Lie, H. et al, 2012, *Comprehensive Riser VIV Model Tests in Uniform and Sheared Flow*, OMAE2012-84055

[5] Tognarelli, M.A. et al, 2004, *VIV Response of a Long Flexible Cylinder in Uniform and Linearly Sheared Currents*, OTC 16338

[6] Crandall, S.H. & Mark, W.D., 1963, *Random Vibration in Mechanical Systems*, Academic Press Inc., New York

[7] WAFO-group, 2006, *WAFO - A Matlab Toolbox for Analysis of Random Waves and Loads - A Tutorial*, Math. Stat., Center for Math Sci., Lund Univ., Lund, Sweden, http://www.maths.lth.se/mathstat/wafo

[8] Fontaine, E. et al, 2011, *Reliability Based Factors of Safety for VIV Fatigue Using NDP Riser High Mode VIV Tests*, OMAE2011-49820

[9] Fontaine, E.R. et al, 2013, *Using Model Test Data to Assess VIV Factor of Safety for SCR and TTR in GOM*, OMAE2013-10984

[10] Rao, Z. et al, 2014, *The Identification of Power-In region in Vortex-Induced Vibration of Flexible Cylinders*, OMAE2014-24472

[11] Resvanis, T.L. & Vandiver, J.K., 2011, *Modelling Risers With Partial Strake Coverage*, OMAE2011-49817

[12] Det Norske Veritas, 2010, *Recommended Practice: Fatigue Design of Offshore Structures*, DNV-RP-C203

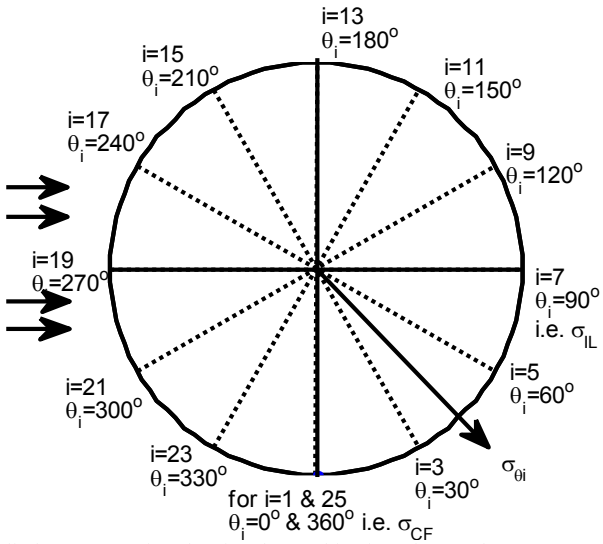

Fig.3 Cylinder cross-section showing the combination of σ_{CF} and σ_{IL}at some arbitrary angle θ_i

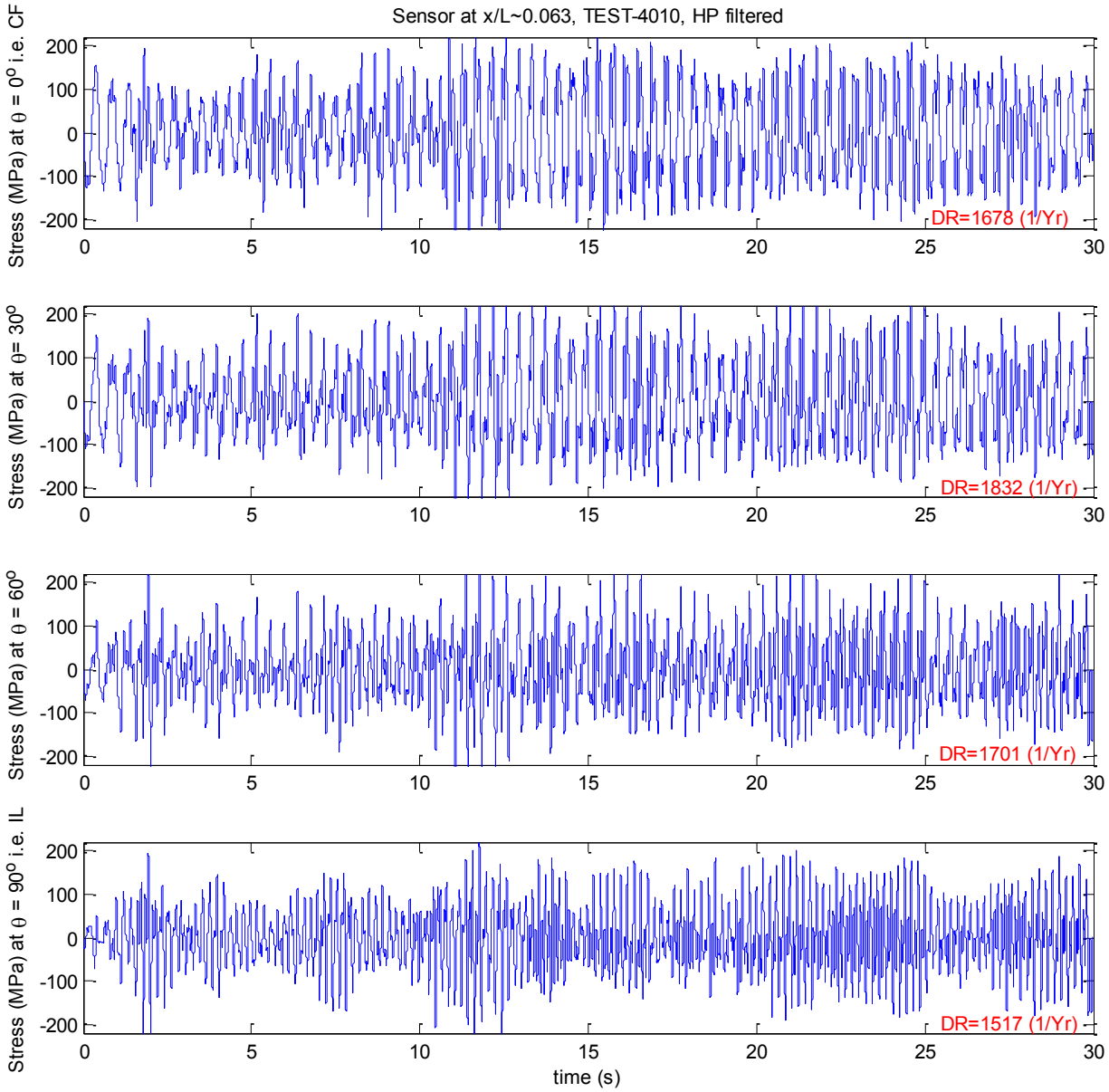

Fig. 4 The stress time-histories at four different locations (θ=0, 30, 60 & 90 degrees) around the circumeference of the cross-section at a position x/L~0.06 along the cylinder length

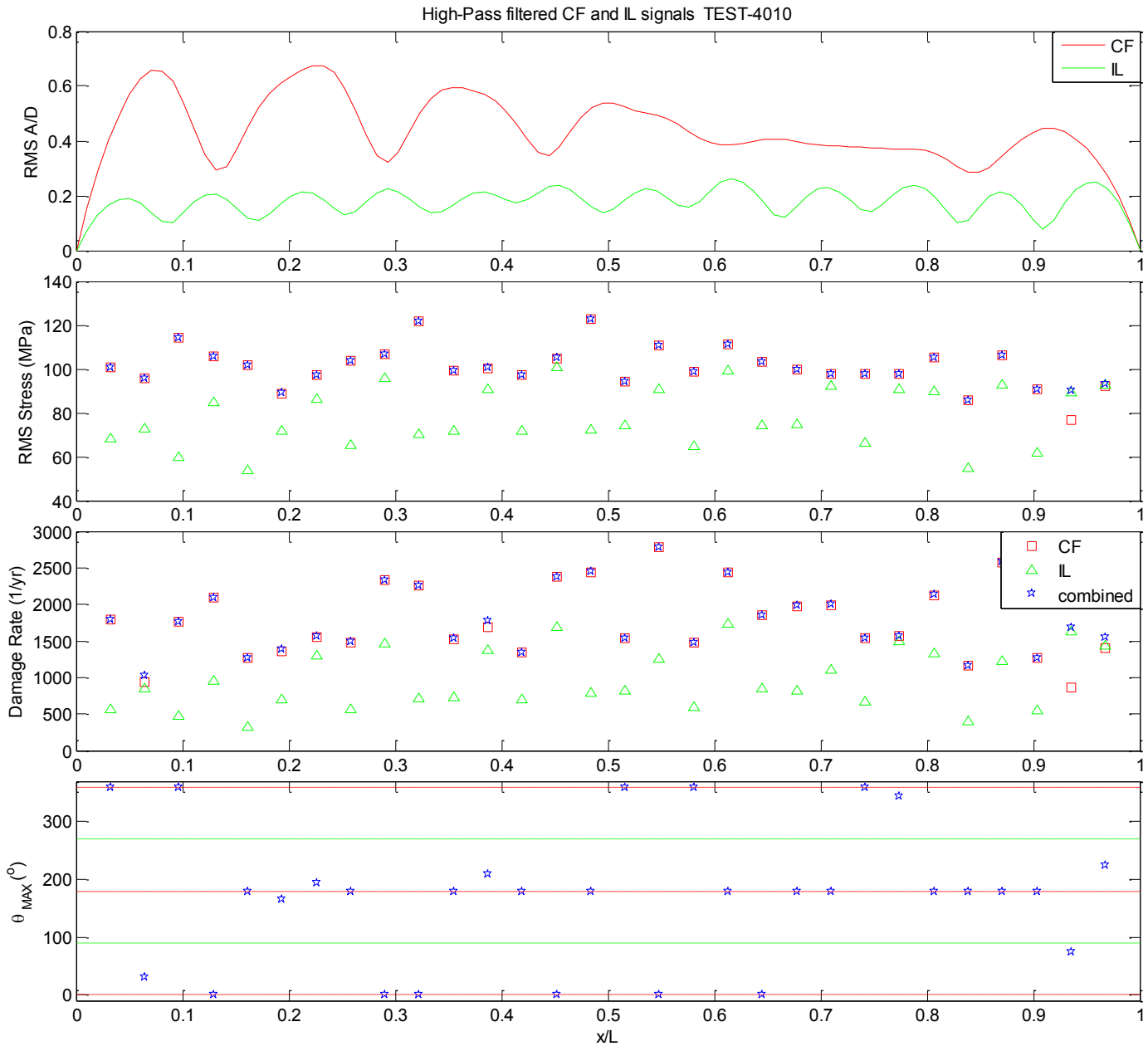

Fig.5 VIV Response under uniform flow conditions of 1.4m/s (test 4010)

Top: CF and IL RMS response amplitude (dimensionless)

2nd from top: CF and IL RMS stresses (MPa) and the largest combination of the signals in both directions

3rd from top: CF and IL damage rates (1/yr) and the most damaging combination of the signals in both directions

Bottom: Angle around the circumference of the cross-section where the most damaging combination of CF and IL damage occurs

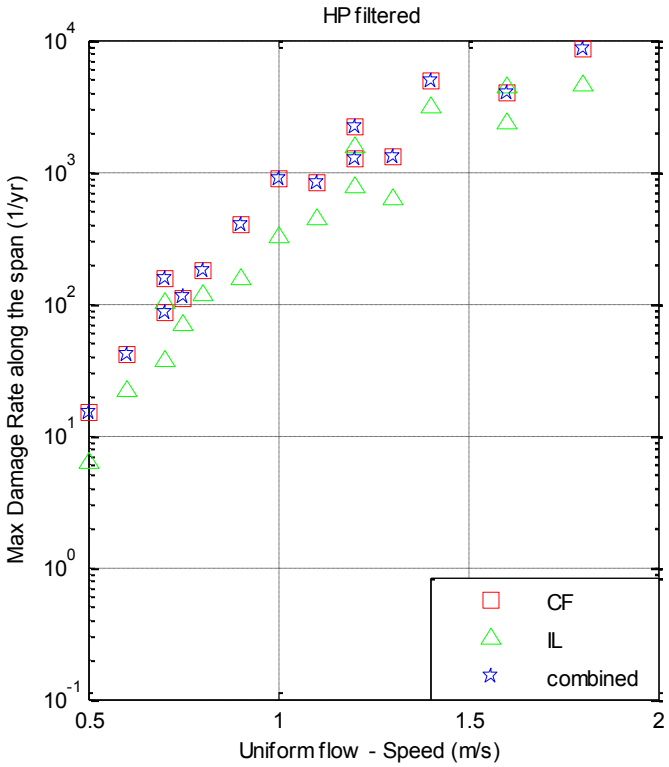

Fig. 6 Maximum Damage Rate (1/yr) vs. towing speed(m/s) in uniform flows. Data shown **includes** all higher harmonics

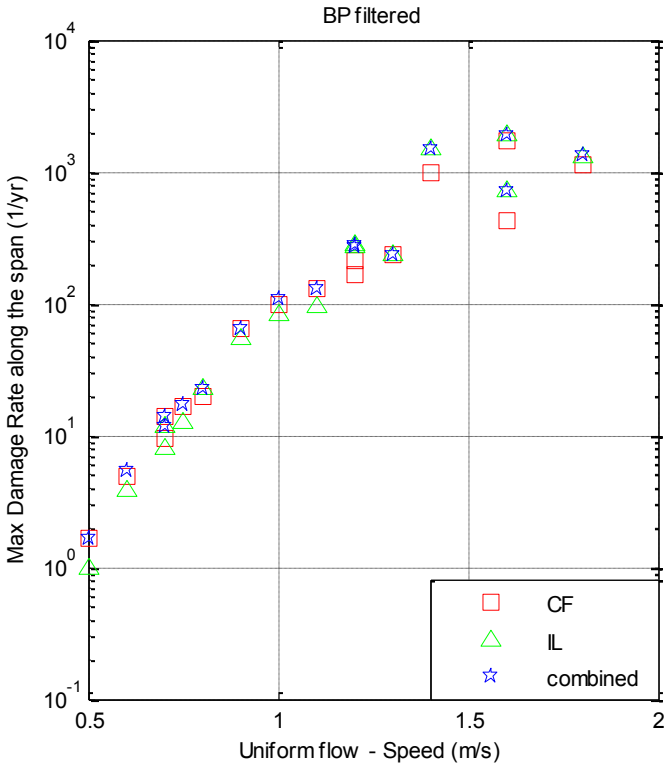

Fig. 8 Maximum Damage Rate (1/yr) vs. towing speed (m/s) in uniform flows. Data shown **excludes** all higher harmonics

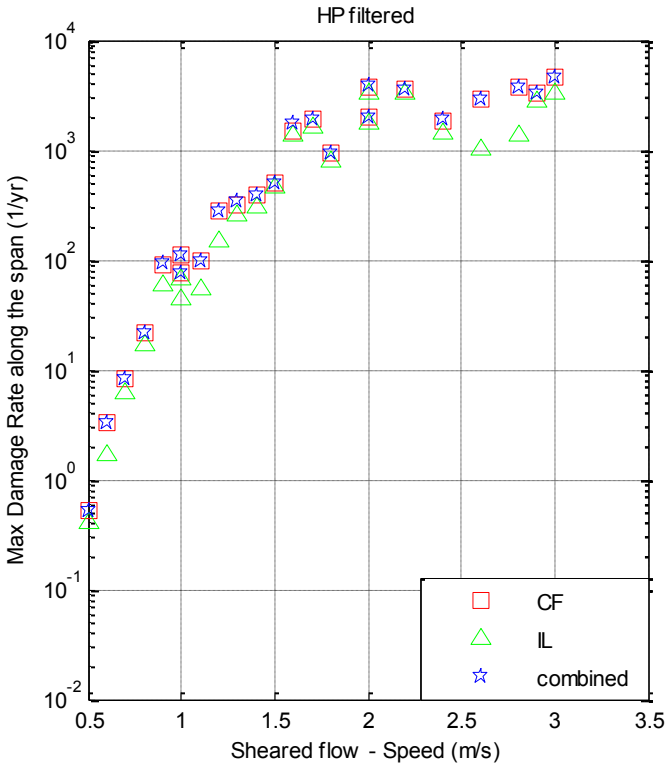

Fig. 7 Maximum Damage Rate (1/yr) vs. towing speed (m/s) in sheared flows. Data shown **includes** all higher harmonics

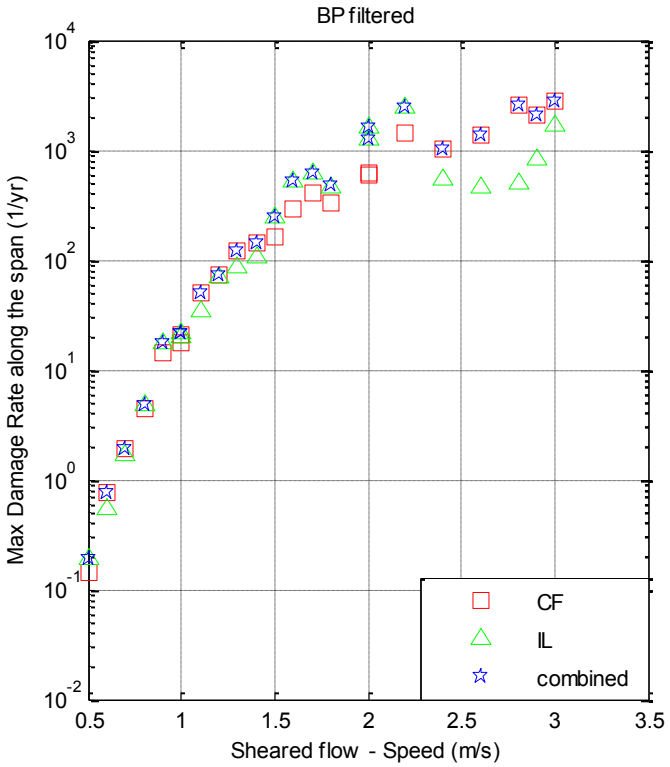

Fig. 9 Maximum Damage Rate (1/yr) vs. towing speed (m/s) in sheared flows. Data shown **excludes** all higher harmonics

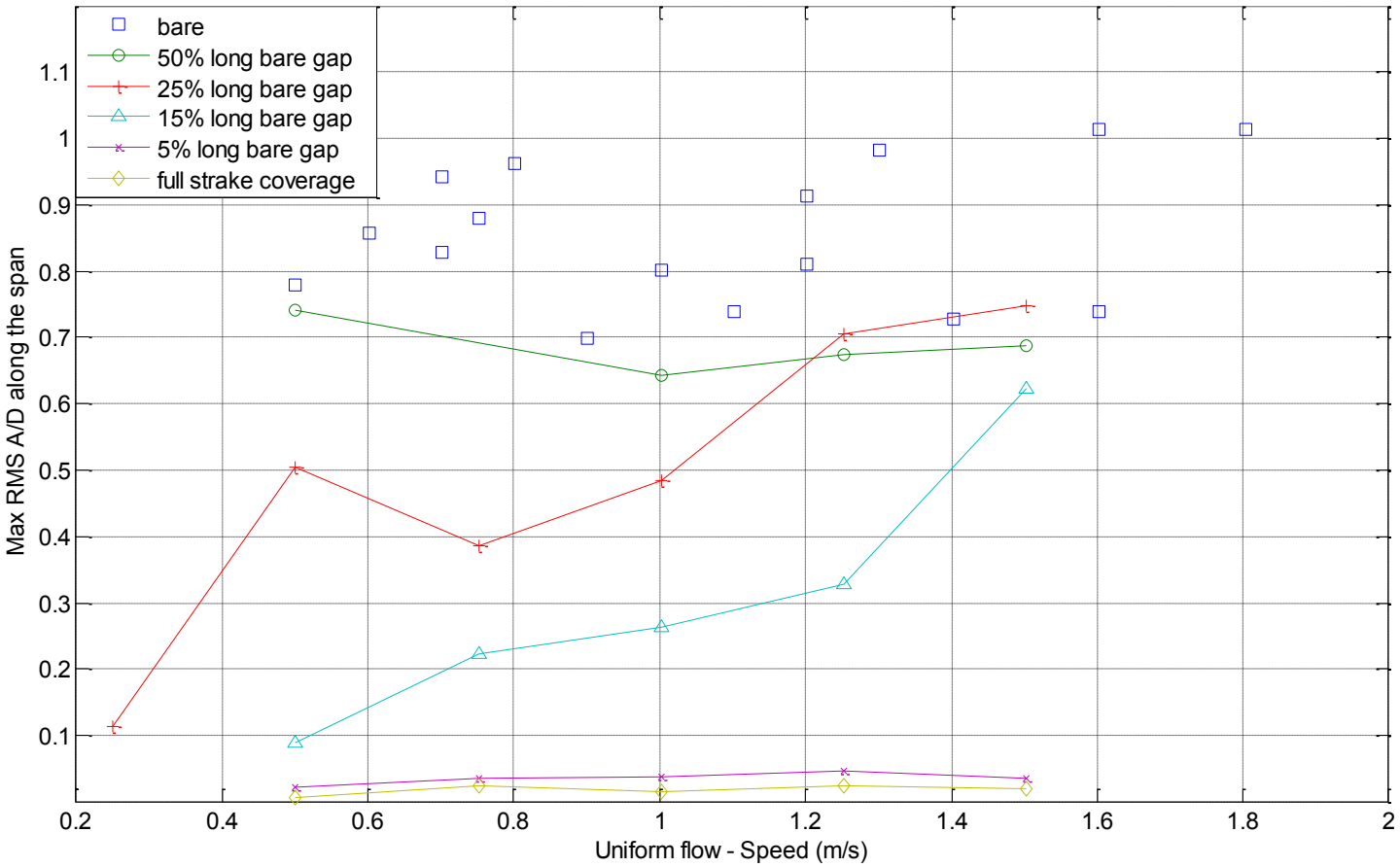

Fig.10 CF RMS Amplitude vs Towing Speed (m/s) in UNIFORM FLOWS

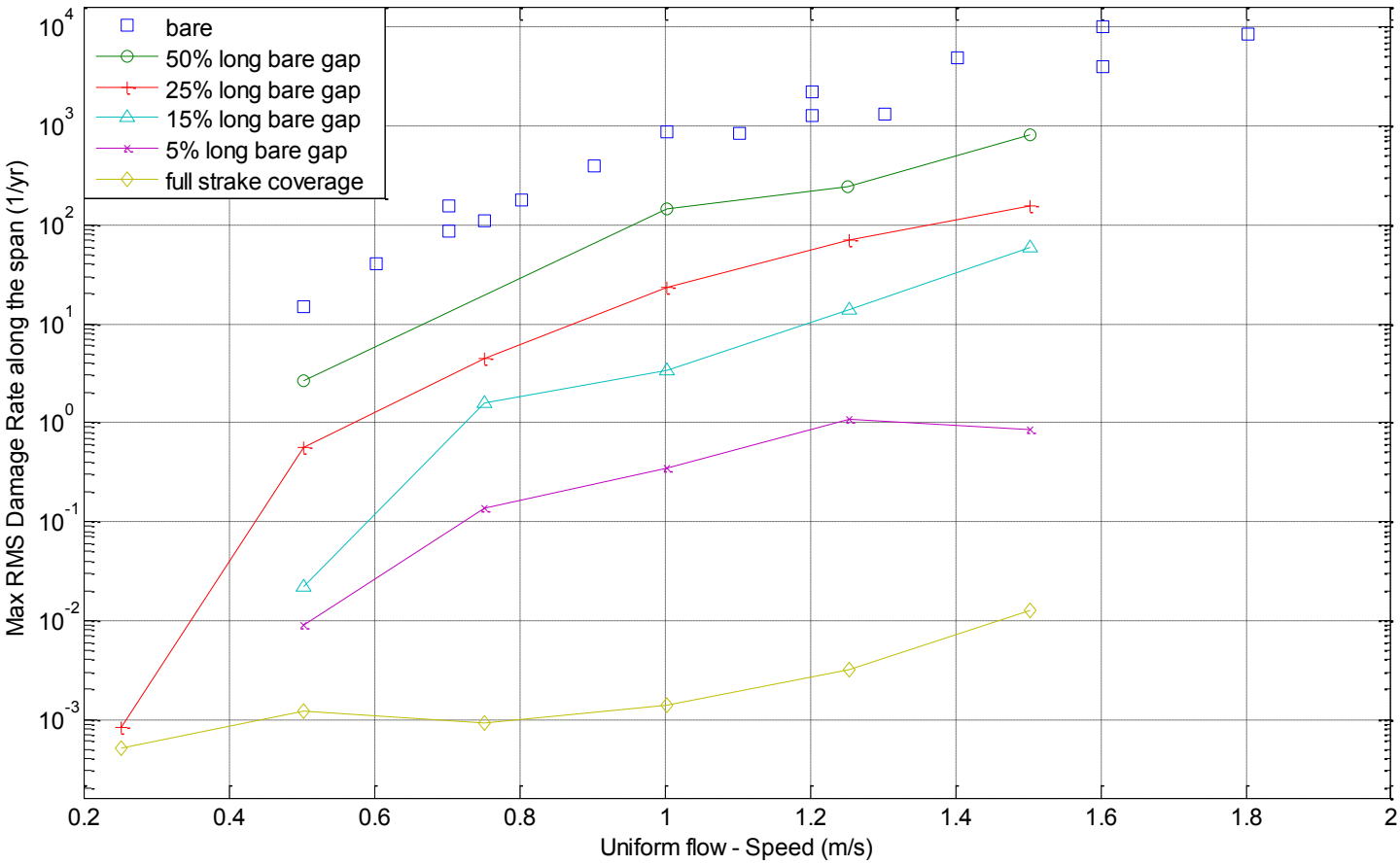

Fig. 11 Maximum Damage Rate (1/yr) vs Towing Speed (m/s) in UNIFORM FLOWS

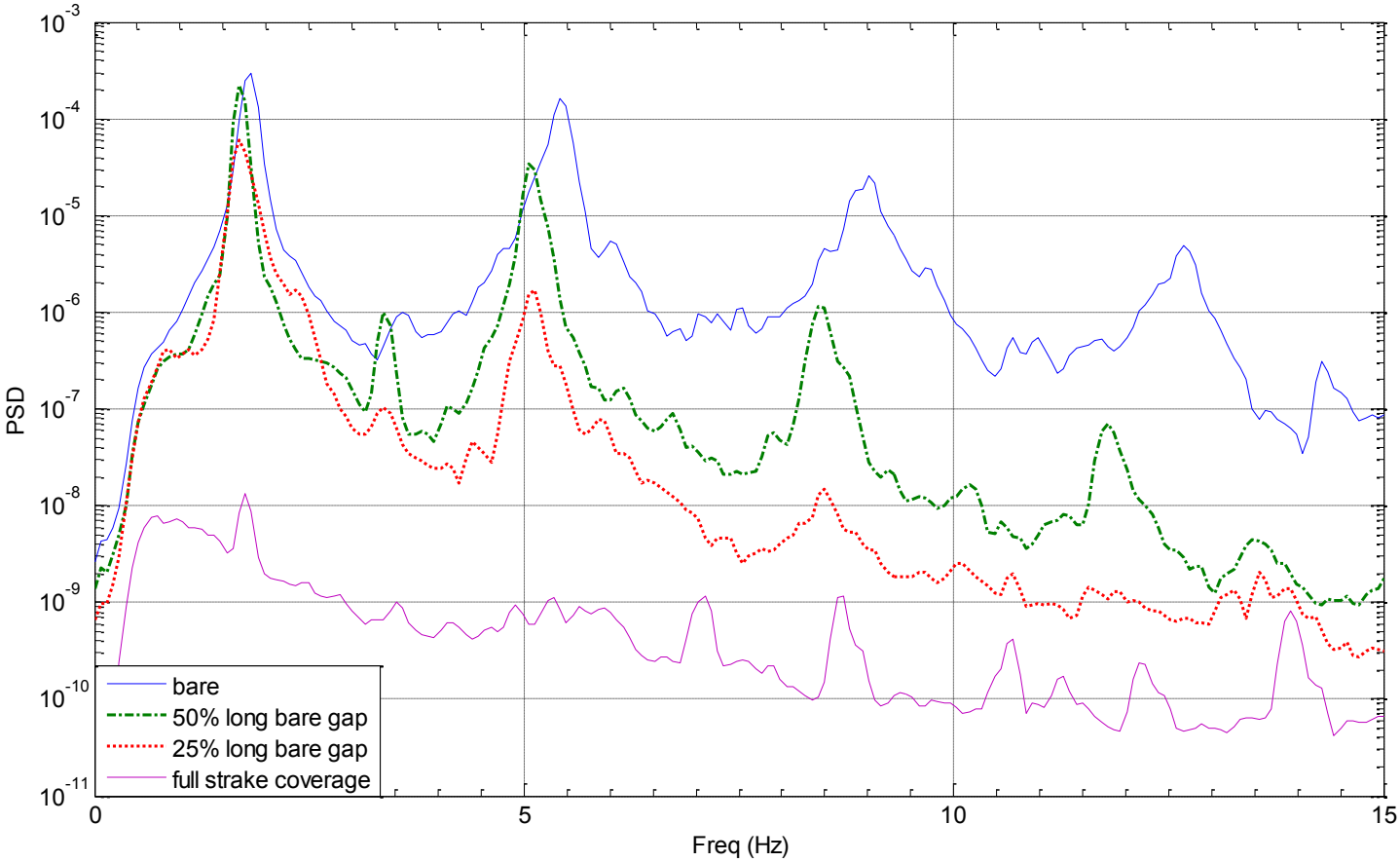

Fig. 12 Averaged Power Spectral Density from all CF sensors for uniform flow of 1m/s

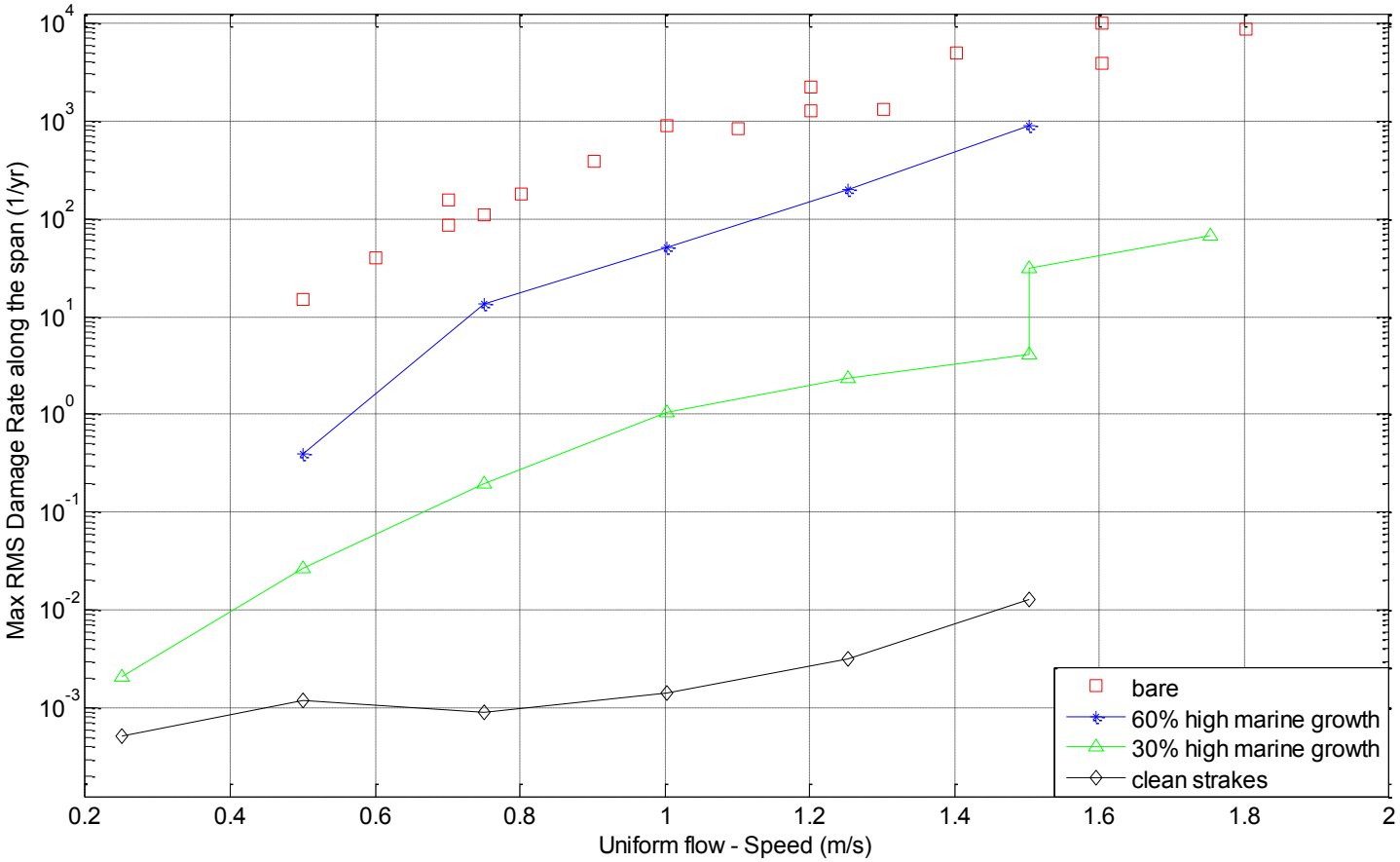

Fig. 13 Maximum Damage Rate (1/yr) vs Towing Speed (m/s) in UNIFORM FLOWS

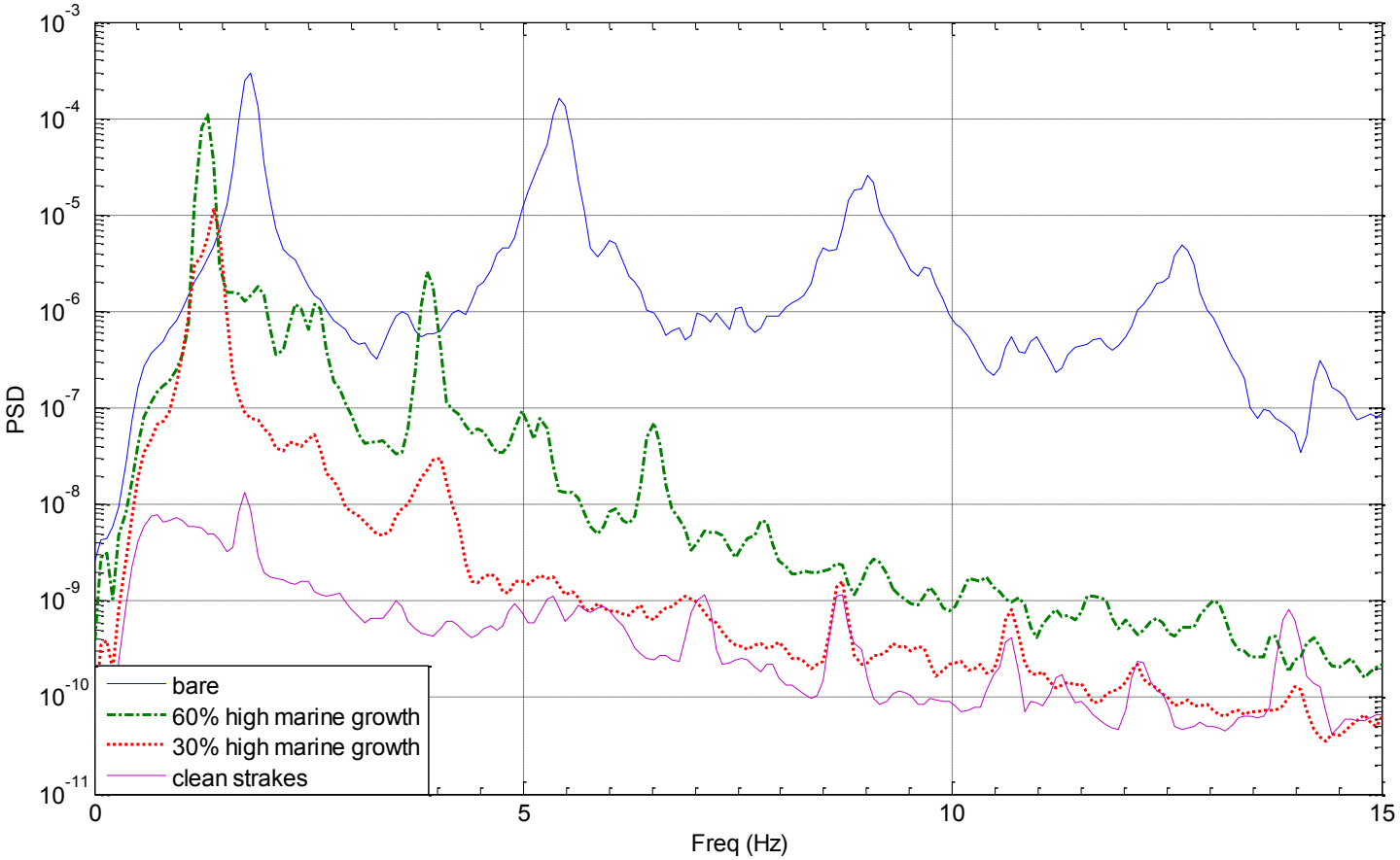

Fig. 14 Averaged Power Spectral Density from all CF sensors for uniform flow of 1m/s

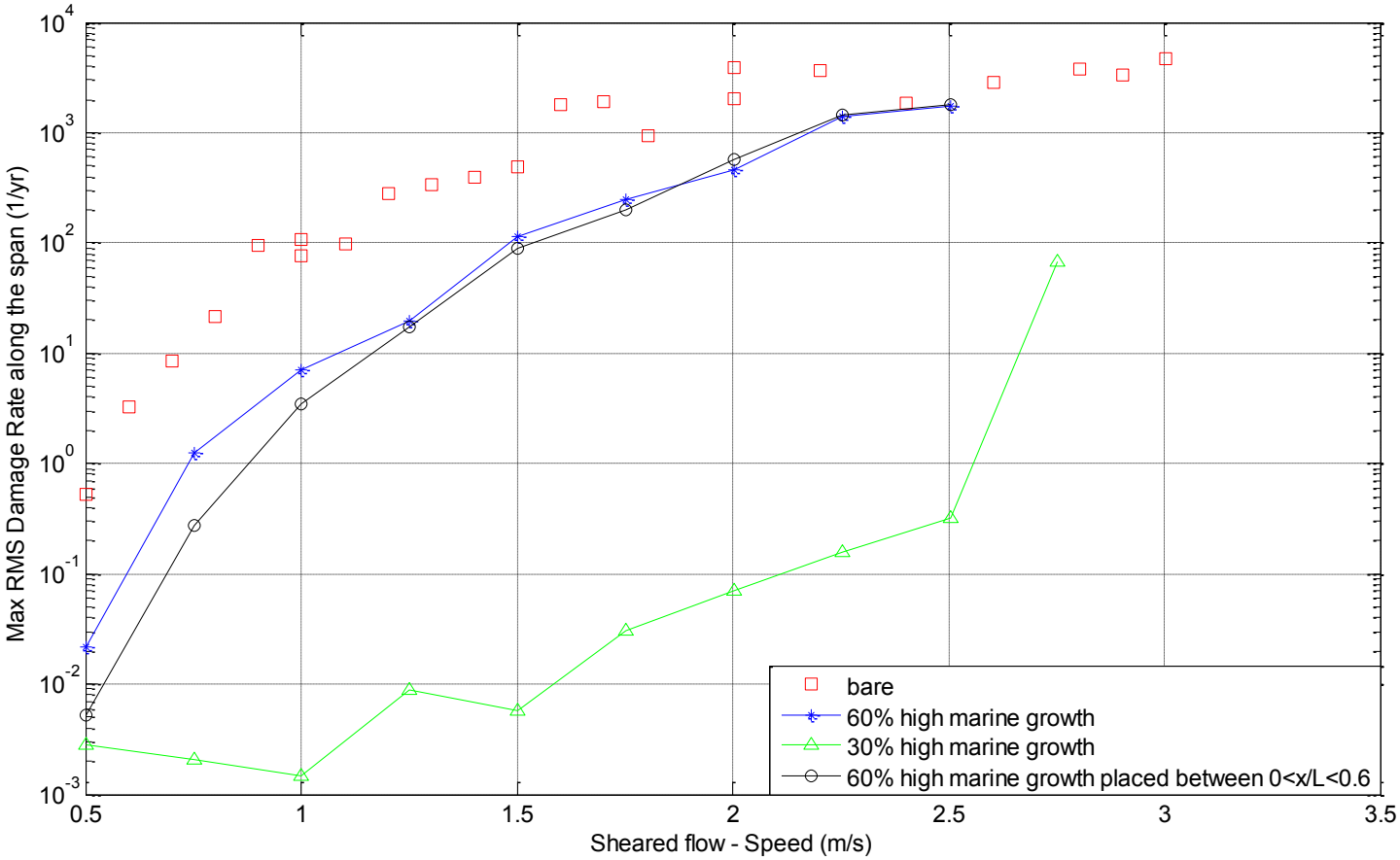

Fig. 15 Maximum Damage Rate (1/yr) vs Towing Speed (m/s) in SHEARED FLOW